Int. J. Heat Mass Transfer. Vol. 35, No. 12, pp. 3323–3333, 1992
Printed in Great Britain

0017–9310/92 $5.00 + 0.00

Rigorous development for radiation heat transfer in nonhomogeneous absorbing, emitting and scattering media

DONALD V. WALTERS
McDonnell Aircraft Company, New Aircraft Products Division, P.O. Box 516, St. Louis, MO 63166-0516, U.S.A.

and

RICHARD O. BUCKIUS
University of Illinois at Urbana–Champaign, Department of Mechanical and Industrial Engineering, 1206 W. Green Street, Urbana, IL 61801, U.S.A.

(*Received* 24 *September* 1991 *and in final form* 10 *January* 1992)

Abstract—In this study, a comprehensive methodology is developed for computing the radiative emission of a generalized enclosure containing an absorbing, emitting, scattering medium. The principle of reciprocity in radiative transfer provides the basis for a reverse Monte Carlo solution for the emission. The result is an approach founded upon complete paths through the enclosure. These paths constitute a generalization of the line-of-sight concept to include the effects of scattering and boundary reflection. Line-of-sight based models for gas absorption can then be incorporated without approximation. Sample results for the emission from a nonhomogeneous, nonisothermal cylindrical medium containing gray particles and a real gas are included.

1. INTRODUCTION

RADIATION heat transfer analyses have advanced greatly over the past several decades. The state-of-the-art has progressed from the analysis of homogeneous, isothermal enclosures that are of simple geometry and which contain nonscattering constituents, to the treatment of multidimensional enclosures with nonhomogeneous, nonisothermal, absorbing, emitting, and scattering constituents. Yet, as refined as some of the newer techniques are, they are incapable of rigorously treating problems with such simple caveats as a nontrivial boundary shape, arbitrary boundary reflectivities, arbitrary scattering phase functions, or path length-dependent gas-band models.

Monte Carlo (MC) methods represent the only technique capable of easily incorporating almost any desired radiative feature. This approach is especially attractive since the time required to formulate an MC model for a particular application is often very brief, since the level of description is simple relative to the more mathematically-based approaches. The effort required to alter the algorithm to accommodate, say, a new boundary shape is also minimal. Of course, the advantage of flexibility that MC methods enjoy is balanced somewhat by their computational expense.

The focus of this study is the reverse Monte Carlo technique, which is based upon the principle of reciprocity in radiative transfer theory as described by Case [1]. The application of the principle for our purpose results in the ability to exactly compute the flux or intensity at a point (differential detector area dA) and do so very efficiently. This is accomplished by tracking bundles in a time-reversed manner from an area element dA into the medium, rather than from the medium to dA, as in conventional 'forward' MC solutions.

The reverse MC method is applied by Gordon [2] in a manner similar to that presented here and in a slightly different fashion by Collins *et al.* [3] and Adams and Kattawar [4]. However, in these cases, volumetric emission is not introduced, and the line-of-sight form for each path's contribution to the intensity is not discussed. These references restrict themselves to the calculation of reflection or transmission of incident energy at a boundary to a small detector. In the computer graphics field, ray-tracing, which is a simplified form of reverse Monte Carlo, has been extended to account for scattering of energy from light sources into the observer's line-of-sight [5–8]. However, none of these studies contribute formulations that introduce distinct paths as the basis for the energy transfer, as is done here.

Several other applications of reverse MC appear in the literature. Notably, Edwards [9] discusses the calculation of intensity at a point within a gaseous medium with diffuse or specular walls. He presents the solution in terms of a zig-zag gaseous path through the medium, as will be done in this study. However, the approach is only briefly mentioned, and its rigorous extension to a generalized medium, especially one with scattering constituents, is not apparent. Recently, Reardon *et al.* [10] and Nelson [11] apply a reverse MC algorithm to evaluate radiative emission

NOMENCLATURE

a	absorption coefficient [m^{-1}]
a_λ	spectral absorption coefficient [m^{-1}]
A	area [m^2]
A_s	total surface area of the boundary [m^2]
dA	area element at which the flux or intensity is evaluated [m^2]
dA_s	surface area element [m^2]
D	cylinder diameter [m]
i	total intensity [W m^{-2} sr^{-1}]
i_b	total black-body intensity [W m^{-2} sr^{-1}]
i_λ	spectral intensity [W μm^{-1} m^{-2} sr^{-1}]
$i_{\lambda b}$	spectral black-body intensity [W μm^{-1} m^{-2} sr^{-1}]
l	photon path length [m]
l_{m1}	photon path length for the end of a path segment nearest $l = 0$ [m]
l_{m2}	photon path length for the end of a path segment furthest from $l = 0$ [m]
L	height of cylinder [m]
L_{mb}	surface area average mean beam length, $4V/A_s$ [m]
M	number of homogeneous cells which compose a nonhomogeneous emission path
$\mathbf{n}$	normal vector
N	number of bundles
P	phase function
$q^{\pm}$	total flux received at area element dA [W m^{-2}]
$q_\lambda^{\pm}$	spectral flux received at dA [W μm^{-1} m^{-2}]
r	radial coordinate of the cylinder [m]
$\mathbf{r}$	location in the enclosure
R	random number on (0, 1)
S_λ	spectral internal source [W μm^{-1} m^{-3} sr^{-1}]
T	temperature [K]
V	total medium volume [m^3]
x	one coordinate of the (x, y, z) system [m]
y	one coordinate of the (x, y, z) system [m]
z	axial coordinate for the cylinder [m], one coordinate of the (x, y, z) system [m], layer coordinate normal to the boundaries [m].

Greek symbols

β	extinction coefficient, $(a+\sigma)$ [m^{-1}]
ε	emissivity
θ	polar angle
κ	optical depth
λ	wavelength [μm]
ρ	reflectivity
σ	scattering coefficient [m^{-1}]
φ	circumferential angle
ω	scattering albedo, $\sigma/(a+\sigma)$
$\mathbf{\Omega}$	vector direction in the enclosure (ξ, η, μ).

Subscripts

ave	average
b	black-body
dh	directional in-hemispherical out
i	internal
in	incoming quantity
inc	incident quantity
k	bundle number
λ	wavelength-dependent quantity
m	length bin number
max	maximum
mb	mean beam length quantity
out	outgoing quantity
s	surface quantity
w	wall
1	first problem of Case's development
2	second problem of Case's development
*	transformed path length.

Superscripts

+	positive direction
−	negative direction
′	directional quantity, incoming direction for scattering
″	bi-directional quantity.

from scattering rocket plumes. However, their approach decouples the absorption and emission processes, a characteristic with practical disadvantages.

In this study, Case's formulation of the reciprocity principle is applied to account for both boundary and volumetric contributions to the emitted flux or intensity at a point. The distinguishing element of the development given here is that complete paths through the absorbing, emitting, and scattering medium are involved. The result is a solution founded upon a set of ray paths which generalize the concept of the line-of-sight to include the effects of scattering and boundary reflection. The emission/absorption process is thus conveniently structured as a synergistic path phenomenon, in contrast to models which consider the emission of energy from a distribution of sources and the subsequent absorption of that energy by the medium as uncoupled phenomena.

This quality is especially important when one wishes to compute the emission from absorbing, emitting, and scattering media and incorporate, in an accurate manner, the behavior of real gases. Accurate models for gas absorption/emission, for example the narrow-band [12] and wide-band [13] models, have been

developed but have the disadvantage that the spectral absorption coefficient is not directly defined. Rather, band quantities which account for the action of many absorption lines in a spectral band are applied. Incorporating the band models into a solution generally requires a rigorous inclusion of the path length dependence. The ray path-based, reverse MC technique is ideally suited for this requirement. In contrast, most solution techniques include the band models by defining for each gas band a mean absorption coefficient based on some length scale, usually the mean beam length L_{mb}, despite the fact that this length is devoid of meaning in a scattering medium. Obtaining the total emission entails solving the radiative transfer equation for each spectral block or band. Such a procedure has been applied and discussed by Mengüc and Viskanta [14, 15]. As these authors note, the error introduced into such solutions by the gray-band approximation can be significant. Another difficulty is that the gas absorption is not even qualitatively represented properly [13].

For radiative transfer solutions in scattering media, the only technique (other than the reverse MC method studied here) available in the literature that is capable of rigorously incorporating the path length-dependent gas-band models is the photon path length method, originally developed by Irvine [16] and extended to heat transfer applications by Buckius and co-workers [17–20]. This approach involves calculating all possible path lengths of the photons in a given medium. Once the distribution of path lengths is found at a given location, any absorption feature is included as a simple integration over path length. Such a radiative transfer solution is exact. Because the functional dependence on path length is explicitly derived, gas absorption and emission in a scattering medium can be accounted for using the exponential wide-band model or other gas-band models without approximation. While the photon path length technique provides solutions for such problems, the complexity of the resultant analytical equations is significant, even for the homogeneous layer. For arbitrary geometries, obtaining an analytical photon path length solution is prohibitive.

In addition to the difficulty of incorporating gas phenomena rigorously, radiative transfer solutions must also be able to account for nonhomogeneity, nonisothermality, reflecting boundaries, and anisotropic scattering. Much work has been performed on solutions to incorporate the effects noted above [21–30]. However, none of these methods are comprehensive in their ability to address all of the following: arbitrary geometry, nonhomogeneity, nonisothermality, anisotropically scattering particles, reflecting walls with an arbitrary reflectivity, and rigorous inclusion of path length-dependent real gas models. Significantly, the reverse MC approach allows the incorporation of all of these effects. The discussion to follow presents this approach in a form which allows incorporation of the path length-dependent absorption models for real gases for the case of a medium which also contains absorbing, emitting, scattering particles. After providing several test cases to demonstrate the validity of the approach for multidimensional, nonhomogeneous, nonisothermal, scattering media, the reverse MC concept is applied to a multidimensional, nonhomogeneous, nonisothermal, scattering medium containing both particles and a real gas to demonstrate the efficacy of the technique. The importance of nonhomogeneity and scattering to such problems is highlighted.

2. SOLUTION DEVELOPMENT

The medium to be treated is an arbitrarily shaped enclosure with absorbing, emitting, reflecting walls containing an isotropic, absorbing, emitting, scattering medium, as illustrated in Fig. 1. For generality, the analysis will be considered on a spectral basis; this will be relaxed later. The enclosure walls are, in general, nonuniform both in temperature $T(\mathbf{r}_s)$ and bi-directional reflectivity $\rho''_\lambda(\mathbf{r}_s, \mathbf{\Omega}_{in}, \mathbf{\Omega}_{out})$. The directional emissivity is $\varepsilon'_\lambda(\mathbf{r}_s, \mathbf{\Omega}) = 1 - \rho'_{\lambda dh}(\mathbf{r}_s, -\mathbf{\Omega})$ with $(\mathbf{n}\cdot\mathbf{\Omega}) > 0$; $\rho'_{\lambda dh}(\mathbf{r}_s, \mathbf{\Omega})$ is the directional in-hemispherical out reflectivity with $(\mathbf{n}\cdot\mathbf{\Omega}) < 0$. $\mathbf{r}_s$ is the location of a differential wall element dA_s, and $\mathbf{\Omega}_{in}$ and $\mathbf{\Omega}_{out}$ are incoming and outgoing directions. Also, θ is a polar angle, φ is a circumferential angle, and $\mathbf{n}$ is the surface normal vector at dA_s, assumed positive when directed into the enclosure. (Note that $\mathbf{\Omega}$ is a unit vector described by $\mathbf{\Omega} = (\xi, \eta, \mu)$, where $\xi = \sin\theta\cos\varphi$, $\eta = \sin\theta\sin\varphi$, and $\mu = \cos\theta$). The participating medium has a temperature $T(\mathbf{r})$, scattering coefficient $\sigma_\lambda(\mathbf{r})$, absorption coefficient $a_\lambda(\mathbf{r})$, and phase function $P_\lambda(\mathbf{r}, \mathbf{\Omega}, \mathbf{\Omega}')$ with $\mathbf{r}$ denoting the medium location. Scattering is assumed to be coherent. The phase function describes scattering from $\mathbf{\Omega}'$ to $\mathbf{\Omega}$, and the integral of P_λ over all incident angles and the integral over all outgoing angles are equal to 4π. Also, $P_\lambda(\mathbf{r}, \mathbf{\Omega}, \mathbf{\Omega}') = P_\lambda(\mathbf{r}, -\mathbf{\Omega}', -\mathbf{\Omega})$; that is, the phase function is time-reversal symmetric. Clearly, the medium is quite generalized, although effects such as dependent scattering, polarization, and medium anisotropy are not considered.

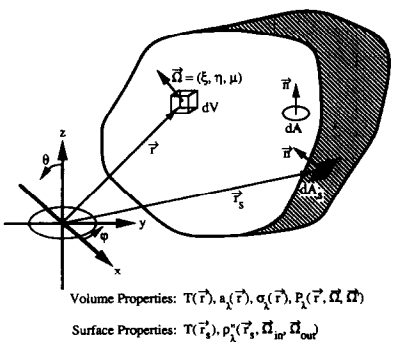

FIG. 1. Multidimensional enclosure with an absorbing, emitting, reflecting boundary and absorbing, emitting, scattering constituents.

Intensity formulation

Radiative heat transfer in a participating medium essentially involves solving, for the above enclosure, the integro-differential radiative transfer equation,

$$(\nabla\cdot\boldsymbol{\Omega})i_\lambda(\mathbf{r},\boldsymbol{\Omega}) = S_\lambda(\mathbf{r},\boldsymbol{\Omega}) - [a_\lambda(\mathbf{r})+\sigma_\lambda(\mathbf{r})]i_\lambda(\mathbf{r},\boldsymbol{\Omega}) + \frac{\sigma_\lambda(\mathbf{r})}{4\pi}\int_{4\pi} P_\lambda(\mathbf{r},\boldsymbol{\Omega},\boldsymbol{\Omega}')i_\lambda(\mathbf{r},\boldsymbol{\Omega}')\,\mathrm{d}\boldsymbol{\Omega}' \quad (1)$$

along with the appropriate boundary conditions. In equation (1), $i_\lambda(\mathbf{r},\boldsymbol{\Omega})$ is the spectral intensity, and S_λ describes the internal source. For the medium described above, S_λ represents volumetric emission with $S_\lambda = a_\lambda(\mathbf{r})i_{\lambda b}(T(\mathbf{r}))$, where $i_{\lambda b}$ is the black-body intensity at temperature T. Conventional MC approaches to solving equation (1) require a direct simulation of the physical processes involved. That is, photon bundles arise from internal sources and from any boundary emitter and proceed to interact with the medium in a stochastic fashion, undergoing absorption, scattering, and reflection processes according to the appropriate cumulative probability density functions. The result in most heat transfer applications is the flux or intensity distribution within the medium and at the boundary.

To develop the necessary expressions for the reverse MC principle, consider two problems as related in the development of Case [1]. Let $i_{\lambda 1}(\mathbf{r},\boldsymbol{\Omega})$ denote the solution to the following radiative transfer problem in the enclosure of volume V:

$$(\nabla\cdot\boldsymbol{\Omega})i_{\lambda 1}(\mathbf{r},\boldsymbol{\Omega}) = S_{\lambda 1}(\mathbf{r},\boldsymbol{\Omega}) - \beta_\lambda(\mathbf{r})i_{\lambda 1}(\mathbf{r},\boldsymbol{\Omega}) + \frac{\sigma_\lambda(\mathbf{r})}{4\pi}\int_{4\pi} P_\lambda(\mathbf{r},\boldsymbol{\Omega},\boldsymbol{\Omega}')i_{\lambda 1}(\mathbf{r},\boldsymbol{\Omega}')\,\mathrm{d}\boldsymbol{\Omega}'. \quad (2)$$

$S_{\lambda 1}(\mathbf{r},\boldsymbol{\Omega})$ is the internal source distribution and $\beta_\lambda = a_\lambda+\sigma_\lambda$. At the enclosure boundary of total area A_s

$$i_{\lambda 1}(\mathbf{r},\boldsymbol{\Omega}) = i_{\lambda 1\mathrm{inc}}(\mathbf{r},\boldsymbol{\Omega}) \quad (3)$$

for $\mathbf{r}$ on A_s and $(\mathbf{n}\cdot\boldsymbol{\Omega}) > 0$, since the surface normal is taken to be directed into the enclosure. Similarly, consider a second solution, $i_{\lambda 2}(\mathbf{r},\boldsymbol{\Omega})$, to the problem

$$(\nabla\cdot\boldsymbol{\Omega})i_{\lambda 2}(\mathbf{r},\boldsymbol{\Omega}) = S_{\lambda 2}(\mathbf{r},\boldsymbol{\Omega}) - \beta_\lambda(\mathbf{r})i_{\lambda 2}(\mathbf{r},\boldsymbol{\Omega}) + \frac{\sigma_\lambda(\mathbf{r})}{4\pi}\int_{4\pi} P_\lambda(\mathbf{r},\boldsymbol{\Omega},\boldsymbol{\Omega}')i_{\lambda 2}(\mathbf{r},\boldsymbol{\Omega}')\,\mathrm{d}\boldsymbol{\Omega}' \quad (4)$$

$$i_{\lambda 2}(\mathbf{r},\boldsymbol{\Omega}) = i_{\lambda 2\mathrm{inc}}(\mathbf{r},\boldsymbol{\Omega}), \quad (\mathbf{n}\cdot\boldsymbol{\Omega}) > 0 \quad \text{and} \quad \mathbf{r} \text{ on } A_s. \quad (5)$$

Case demonstrates that these solutions are related by the following identity:

$$\int_{A_s}\int_{(\mathbf{n}\cdot\boldsymbol{\Omega})>0}\{(\mathbf{n}\cdot\boldsymbol{\Omega})[i_{\lambda 2\mathrm{inc}}(\mathbf{r},\boldsymbol{\Omega})i_{\lambda 1}(\mathbf{r},-\boldsymbol{\Omega}) - i_{\lambda 1\mathrm{inc}}(\mathbf{r},\boldsymbol{\Omega})i_{\lambda 2}(\mathbf{r},-\boldsymbol{\Omega})]\}\,\mathrm{d}\boldsymbol{\Omega}\,\mathrm{d}A_s = \int_V\int_{4\pi}[i_{\lambda 2}(\mathbf{r},-\boldsymbol{\Omega})S_{\lambda 1}(\mathbf{r},\boldsymbol{\Omega}) - i_{\lambda 1}(\mathbf{r},\boldsymbol{\Omega})S_{\lambda 2}(\mathbf{r},-\boldsymbol{\Omega})]\,\mathrm{d}\boldsymbol{\Omega}\,\mathrm{d}\mathbf{r}. \quad (6)$$

This equation presupposes that the scattering phase function satisfies

$$P_\lambda(\mathbf{r},\boldsymbol{\Omega},\boldsymbol{\Omega}') = P_\lambda(\mathbf{r},-\boldsymbol{\Omega}',-\boldsymbol{\Omega}), \quad (7)$$

which implies time reversal symmetry.

Now, consider the enclosure problem posed in relation to Fig. 1. The desired result is the intensity $i_{\lambda 1}(\mathbf{r},\boldsymbol{\Omega})$ at a location $\mathbf{r}$ in direction $\boldsymbol{\Omega}$. Thus, $i_{\lambda 1}$ is the solution given a thermal source and boundary incidence of the form:

$$S_{\lambda 1}(\mathbf{r},\boldsymbol{\Omega}) = a_\lambda(\mathbf{r})i_{\lambda b}(T(\mathbf{r})) \quad (8)$$

and

$$i_{\lambda 1\mathrm{inc}}(\mathbf{r},\boldsymbol{\Omega}) = i_{\lambda b}(T(\mathbf{r})) \quad \text{for } \mathbf{r} \text{ on } A_s \text{ and } (\mathbf{n}\cdot\boldsymbol{\Omega}) > 0. \quad (9)$$

For now, the boundary is assumed to be black with temperature distribution $T(\mathbf{r})$. Now, let $i_{\lambda 2}$ be a solution given the following conditions:

$$S_{\lambda 2}(\mathbf{r},\boldsymbol{\Omega}) = \delta(\mathbf{r}-\mathbf{r}_i)\delta_2(\boldsymbol{\Omega}\cdot\boldsymbol{\Omega}_i) \quad (10)$$

and

$$i_{\lambda 2\mathrm{inc}}(\mathbf{r},\boldsymbol{\Omega}) = 0, \quad (11)$$

where $\delta(\ )$ is the delta function, $\delta_2(\ ) = 0$ when

$$(\boldsymbol{\Omega}\cdot\boldsymbol{\Omega}_i) \neq 0, \quad \int_V \delta(\mathbf{r}-\mathbf{r}_i)\,\mathrm{d}\mathbf{r} = 1,$$

and

$$\int_{4\pi}\delta_2(\boldsymbol{\Omega}\cdot\boldsymbol{\Omega}_i)\,\mathrm{d}\boldsymbol{\Omega} = 1.$$

$S_{\lambda 2}$ corresponds to a collimated source at $\mathbf{r}_i$ emitting unit spectral power into direction $\boldsymbol{\Omega}_i$. The intensity of the beam as it emanates from the source is

$$i_{\lambda 2}(\mathbf{r}_i,\boldsymbol{\Omega}_i) = \frac{\delta_2(\boldsymbol{\Omega}\cdot\boldsymbol{\Omega}_i)}{\mathrm{d}A} \quad (12)$$

where $\mathrm{d}A$ is taken to characterize the cross-sectional area of the collimated ray. Substituting equations (8)–(12) into equation (6) gives

$$i_{\lambda 1}(\mathbf{r}_i,-\boldsymbol{\Omega}_i) = \int_{A_s}\int_{(\mathbf{n}\cdot\boldsymbol{\Omega})>0}[(\mathbf{n}\cdot\boldsymbol{\Omega})i_{\lambda b}(T(\mathbf{r}))i_{\lambda 2}(\mathbf{r},-\boldsymbol{\Omega})]\,\mathrm{d}\boldsymbol{\Omega}\,\mathrm{d}A_s + \int_V\int_{4\pi}[i_{\lambda 2}(\mathbf{r},-\boldsymbol{\Omega})a_\lambda(\mathbf{r})i_{\lambda b}(T(\mathbf{r}))]\,\mathrm{d}\boldsymbol{\Omega}\,\mathrm{d}\mathbf{r}. \quad (13)$$

The intensity $i_{\lambda 1}(\mathbf{r}_i,-\boldsymbol{\Omega}_i)$ for problem 1 at location $\mathbf{r}_i$ in direction $-\boldsymbol{\Omega}_i$ (opposite that of the source emission) is then the sum of an integral over the bounding surface and an integral over the volume.

This last expression is the starting point for the development of the reverse Monte Carlo approach. Note that the unknown quantity in each of the integrals is the solution to problem 2 (or $i_{\lambda 2}$) throughout

the enclosure. The advantage of this relationship is that problem 2 is a simpler problem to solve relative to problem 1 since it involves emission from a single point source rather than from the entire boundary and volume. In terms of the previous discussion, this relationship constitutes a reverse solution for the intensity at a point $i_{\lambda 1}(\mathbf{r}_i, -\mathbf{\Omega}_i)$.

Reverse Monte Carlo development

Monte Carlo now enters as a convenient method for affecting the solution to problem 2. This approach is also particularly useful since it can provide complete paths through the medium, an attribute whose importance will become clear in the development to follow. The solution to problem 2 is accomplished by emitting N rays of energy from the source $(S_{\lambda 2}(\mathbf{r}_i, \mathbf{\Omega}_i))$ at $\mathbf{r}_i$ in direction $\mathbf{\Omega}_i$. Each of the N collimated rays has an initial intensity of the form given by equation (12). After emission, each ray is tracked, in the sense of a Monte Carlo simulation, through the nonemitting medium of problem 2, undergoing scattering events, until intercepting the black enclosure boundary at some location $\mathbf{r}_s$ and direction $\mathbf{\Omega}_s$. The MC technique used during tracking applies absorption suppression whereby scattering interactions determine the bundle's path of travel and the weight of the bundle is exponentially attenuated along the path by absorption only. The length of bundle travel between scattering events and the direction of scatter are determined from the appropriate probability functions using the scattering coefficient and the phase function. An illustration of a complete bundle path is given in Fig. 2.

For N such paths, the intensity $i_{\lambda 1}$, computed using equation (13), is obtained as an average over the N samplings as

$$i_{\lambda 1}(\mathbf{r}_i, -\mathbf{\Omega}_i) = \frac{1}{N}\sum_{k=1}^{N} i_{\lambda 1k}(\mathbf{r}_i, -\mathbf{\Omega}_i). \tag{14}$$

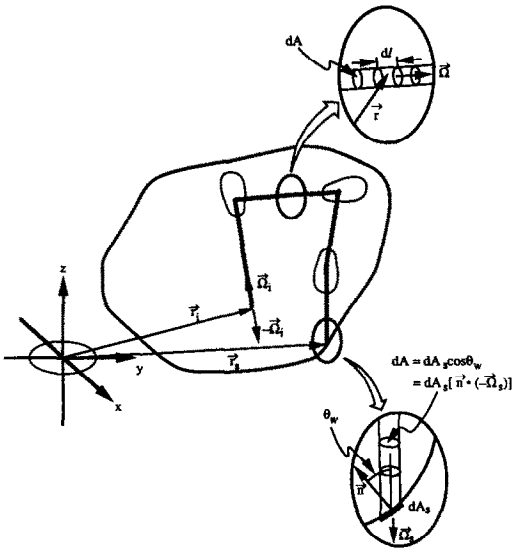

FIG. 2. A complete ray path within the multidimensional enclosure.

The individual $i_{\lambda 1k}$ values are obtained by noting that for an individual ray path, equation (13) reduces to

$$i_{\lambda 1k}(\mathbf{r}_i, -\mathbf{\Omega}_i) = i_{\lambda b}(T(\mathbf{r}_s)) \times \exp\left[-\int_0^{l(\mathbf{r}_s)} a_\lambda(\mathbf{r})\, \mathrm{d}l'(\mathbf{r})\right]\left\{\frac{[\mathbf{n}\cdot -\mathbf{\Omega}_s]\, \mathrm{d}A_s}{\mathrm{d}A}\right\} + \int_0^{l(\mathbf{r}_s)} a_\lambda(\mathbf{r}) i_{\lambda b}(T(\mathbf{r})) \times \frac{\exp\left[-\int_0^{l'(\mathbf{r})} a_\lambda(\mathbf{r})\, \mathrm{d}l''(\mathbf{r})\right]}{\mathrm{d}A} \mathrm{d}A\, \mathrm{d}l'(\mathbf{r}). \tag{15}$$

Referring to Fig. 2, note that only area $\mathrm{d}A_s$ at location $\mathbf{r}_s$ and direction $-\mathbf{\Omega}_s$ contribute to the first integral and the quantity in the brace ($\{\}$) reduces to unity. In the second integral, only those volume elements at positions $\mathbf{r}$ which lie along the ray path with local direction $\mathbf{\Omega}$ contribute. In this equation, $l(\mathbf{r})$ represents the length of travel of the ray when at position $\mathbf{r}$ along the ray path, where $l(\mathbf{r}_i) = 0$. Denoting $l(\mathbf{r}_s) = l_{\max}$ and introducing a change of variable of the form $l_*(\mathbf{r}) = l(\mathbf{r}_s) - l(\mathbf{r})$ allows the integrals in the above equation to proceed from $l_*(\mathbf{r}_s) = 0$ to $l_*(\mathbf{r}_i) = l_{\max}$:

$$i_{\lambda 1k}(\mathbf{r}_i, -\mathbf{\Omega}_i) = i_{\lambda b}(T(\mathbf{r}_s)) \exp\left[-\int_0^{l_{\max}} a_\lambda(\mathbf{r})\, \mathrm{d}l_*(\mathbf{r})\right] + \int_0^{l_{\max}} a_\lambda(\mathbf{r}) i_{\lambda b}(T(\mathbf{r})) \times \exp\left[-\int_{l_*(\mathbf{r})}^{l_{\max}} a_\lambda(\mathbf{r})\, \mathrm{d}l_{**}(\mathbf{r})\right] \mathrm{d}l_*(\mathbf{r}). \tag{16}$$

If the zig-zag path is conceptually removed from the medium and straightened out to form an absorbing, emitting line-of-sight, the expression for $i_{\lambda 1k}$ is seen to be nothing more than that portion of the black wall intensity transmitted to $\mathbf{r}_i$ by the path, added to the line-of-sight emission from the path.

Clearly, the evaluation of the path intensity $i_{\lambda 1k}$ is the most significant element of the solution. To simplify the notation, assume that the ray path, defined with the kth tracking bundle, has a total length l_k, and the absorption coefficient and temperature are known as a function of path length $[T(l), a_\lambda(l)]$, $l' = 0$ is taken to be at the termination point $\mathbf{r}_s$ of the path at the enclosure boundary, $l' = l_k$ is at the location $\mathbf{r}_i$, and T_w is $T(\mathbf{r}_s)$. Equation (16) then becomes

$$i_{\lambda 1k} = \int_0^{l_k} i_{\lambda b}[T(l')] a_\lambda(l') \exp\left[-\int_{l'}^{l_k} a_\lambda(l'')\, \mathrm{d}l''\right] \mathrm{d}l' + i_{\lambda b}(T_w) \exp\left[-\int_0^{l_k} a_\lambda(l')\, \mathrm{d}l'\right]. \tag{17}$$

If the path from $l' = 0$ to $l' = l_k$ is a piecewise homogeneous one through the nonhomogeneous, nonisothermal medium (a practical modeling assump-

tion), the first term in equation (17) is rewritten as a summation over M uniform cells along path l_k:

$$i_{\lambda 1k} = \sum_{m=1}^{M} \left\{ i_{\lambda b}(T_m) \left(\exp\left[-\int_{l_{m2}}^{l_k} a_\lambda(l')\,\mathrm{d}l' \right] - \exp\left[-\int_{l_{m1}}^{l_k} a_\lambda(l')\,\mathrm{d}l' \right] \right) \right\} + i_{\lambda b}(T_w) \exp\left[-\int_0^{l_k} a_\lambda(l')\,\mathrm{d}l' \right]. \quad (18)$$

In this equation, T_m is the temperature of cell m along the ray path, and l_{m1} and l_{m2} define the length boundaries of cell m. l_{m1} is the cell boundary nearest $l' = 0$ (boundary point) and l_{m2} is the cell boundary nearest $l' = l_k$ (location $\mathbf{r}_i$). For a more complex medium containing particles and real gas, developing the equations for path intensity is relatively straightforward.

Thus, an MC simulation of the above, in computing the intensity $i_{\lambda 1}(\mathbf{r}_i, -\mathbf{\Omega}_i)$, considers N ray paths determined from Monte Carlo by ejecting tracking bundles in the $+\mathbf{\Omega}_i$ direction. Each of the tracking bundles is followed through scattering interactions until encountering the black enclosure boundary. At that point, the resultant zig-zag path is considered as a line-of-sight from the black wall, through the *absorbing and emitting* enclosure constituents, back to the point of ejection $\mathbf{r}_i$. Equation (18) is used to compute the path intensity, and the average over-all ray paths in equation (14) gives $i_{\lambda 1}(\mathbf{r}_i, -\mathbf{\Omega}_i)$. Tracing the ray paths is thus equivalent to a time reversal or backward tracking of the photons which contribute to the intensity desired. This is possible precisely because of the time reversal symmetry characteristic of the scattering phase function.

The importance of equation (18) and the corresponding equations involving gases and particles is that all are in terms of transmission quantities $\exp[-\kappa]$ or explicitly involve band quantities, evaluated for a specific, complete path through the enclosure. (Recall that the commonly used gas-band models require a path-based description of the participating medium since gas spectral absorption coefficients are not defined.) Thus, radiative transfer calculations using the ray paths rigorously include all gas effects.

Radiative heat flux calculations

If the calculation of the flux at a point rather than the intensity is desired, the procedure outlined above changes very little. As shown in Fig. 3, the solution for the emitted flux into either the positive or negative hemisphere (relative to the positive normal $\mathbf{n}$) of an element $\mathrm{d}A$ at $\mathbf{r}_i$ is computed by diffusely releasing tracking bundles (in the sense of an MC solution) into the opposite hemisphere to locate the ray paths. (This methodology is the stochastic equivalent of integrating an appropriately weighted directional intensity over the appropriate hemisphere.) The flux is then evaluated as a summation of path intensities. Thus

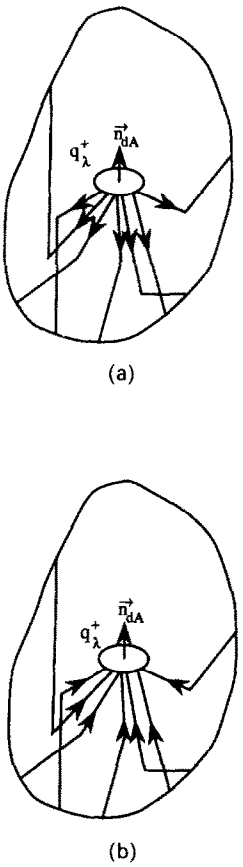

FIG. 3. The computation of the directional flux at an interior area element $\mathrm{d}A$. (a) Tracking bundle paths. (b) Paths for emission.

$$q_{\lambda 1}^{\pm}(\mathbf{r}_i) = \frac{\pi}{N} \sum_{k=1}^{N} i_{\lambda 1k}(\mathbf{r}_i, -\mathbf{\Omega}_{ik}), \quad (19)$$

where $i_{\lambda 1k}$ is computed using equations (16)–(18), $(\mathbf{n}\cdot\mathbf{\Omega}_{ik}) < 0$ for $q_{\lambda 1}^+$, and $(\mathbf{n}\cdot\mathbf{\Omega}_{ik}) > 0$ for $q_{\lambda 1}^-$. The initial direction of the ray path for each intensity calculation is $+\mathbf{\Omega}_{ik}$.

Nonblack boundary conditions

Thus far, the enclosure walls have been considered black, and the boundary's contribution to the path intensity is black-body intensity $i_{\lambda b}$, evaluated at the local wall temperature $T(\mathbf{r}_s)$. If instead the walls are reflecting, it is convenient to view each area $\mathrm{d}A_s$ as conceptually composed of fractional areas that are perfectly reflecting and perfectly absorbing (and emitting). If the surface is diffuse, a fraction $\rho_\lambda(\mathbf{r}_s)$ perfectly reflects and $\varepsilon_\lambda(\mathbf{r}_s) = \alpha_\lambda(\mathbf{r}_s) = 1 - \rho_\lambda(\mathbf{r}_s)$ perfectly absorbs. Thus, when a bundle is tracked to the boundary, a random number R_ρ is generated and compared to $\rho_\lambda(\mathbf{r}_s)$. If $R_\rho < \rho_\lambda(\mathbf{r}_s)$, the ray is reflected diffusely, and its history is continued just as if it had been scattered. If $R_\rho > \rho_\lambda(\mathbf{r}_s)$, the ray path is ended, and the boundary condition for evaluating the path intensity is $i_{\lambda b}(T(\mathbf{r}_s))$. This method implicitly accounts for

reflection and does so in a way which ultimately allows the path intensity to be computed using equation (16)–(18), just as before. The only caveat is that the zig-zag paths now incorporate surface interactions as well as particle scattering.

For a more complex surface, characterized by a bi-directional reflectivity $\rho''_\lambda(\mathbf{r}_s, \boldsymbol{\Omega}_{in}, \boldsymbol{\Omega}_{out})$, the effects of directionally dependent absorptivity, reflectivity, and emissivity must be included. To do so, one again applies the perfectly reflecting, perfectly absorbing concept but on a directional basis. In the following, the bi-directional reflectivity is assumed to have time-reversal symmetry, whereby

$$\rho''_\lambda(\mathbf{r}_s, \boldsymbol{\Omega}_{in}, \boldsymbol{\Omega}_{out}) = \rho''_\lambda(\mathbf{r}_s, -\boldsymbol{\Omega}_{out}, -\boldsymbol{\Omega}_{in}). \quad (20)$$

As a ray path intersects the boundary in some direction $\boldsymbol{\Omega}_{in}$, a random number R_ρ is tested against the directional in-hemispherical out reflectivity, $\rho'_{\lambda dh}(\mathbf{r}_s, \boldsymbol{\Omega}_{in})$. Therefore, the fraction of dA_s that is perfectly reflecting is $\rho'_{\lambda dh}$ for direction $\boldsymbol{\Omega}_{in}$, with the fraction $(1-\rho'_{\lambda dh})$ perfectly absorbing. If reflection occurs, the direction $\boldsymbol{\Omega}_{out}$ is then sampled from the bi-directional reflectivity. Realistic wall interactions therefore introduce little added complexity to the calculation of the path intensity. In fact, the scattering and reflection interactions are treated in a similar fashion. This is directly attributable to the time-reversal symmetry of both the bi-directional reflectivity and the scattering phase function.

Strengths of the reverse MC solution

A primary benefit of the reverse MC solution outlined above is the conceptual understanding it affords. With the solution structured as a set of ray paths, one interpretation to the physical problem is that the scattering and reflection influenced paths are a logical extension of the line-of-sight to scattering, reflecting media. In fact, one can easily demonstrate that for a non-scattering medium with transparent, black boundaries, the ray paths reduce to simple lines-of-sight and, clearly, are valid artifices for calculating the radiative transfer. On an even more fundamental level, the reverse rays allow volumetric radiative emission to be considered as a path phenomenon rather than a volumetric one. Thus, a convenient term to use for the rays is emission paths.

Also, as stated before, the emission paths are invaluable in their ability to return the flux or intensity at a point, exactly (given an infinite number of rays), for an enclosure which contains a real gas in addition to scattering constituents and reflecting surfaces. Since reverse Monte Carlo, unlike most solution techniques, is based upon complete paths through the medium, a direct application of the line-of-sight-based gas-band models is possible. An example of the incorporation of a real gas into an enclosure emission analysis is provided in the next section.

Another strength is that the emission paths are simple geometric entities defined using only the particle scattering coefficient σ_λ, phase function P_λ, and boundary reflectivity ρ''_λ. Over wavelength intervals where σ_λ, P_λ, and ρ''_λ can concurrently be considered gray, a single set of N emission paths is applicable. Generally, the absorption and emission spectra of surfaces and particles are of a much more continuous nature than those of gases, and averaging of particle and surface properties over wavelength intervals large relative to the widths of gas bands is a valid modeling approach. Thus, the number of necessary spectral radiative transfer solutions is significantly reduced when evaluating a wavelength-integrated flux or intensity for a problem involving real gases. With gray particles and surfaces, one set of N ray paths applies for all wavelengths.

3. RESULTS

Several test cases and representative results for gas–particle media are now presented to demonstrate the reverse Monte Carlo (emission path) concept. The computer code written to apply the methodology described above is capable of returning the medium-emitted flux or normal intensity at any location on the boundary of an axisymmetric cylinder. The scattering medium may be nonhomogeneous and nonisothermal and may contain both gray particles and real gases (CO_2 and H_2O). Wide-band modeling and nonhomogeneous scaling of the wide-band parameters [13] are used to describe the gas absorption and emission. The azimuthally symmetric, anisotropic particle phase function is taken to be independent of incident direction. The boundaries of the medium have a uniform temperature T_w and are either black or diffuse and gray.

Test cases

For the test cases presented here, attention is restricted to a nonhomogeneous, nonisothermal, isotropically scattering, gray-particle medium with transparent boundaries, and the total medium-emitted flux to area elements on the boundary is computed. Where possible, comparisons against reported values in the literature are performed. Otherwise, a forward MC code, which applies a straightforward volumetric emission methodology, is used to obtain the radiative flux at boundary locations of planar and cylindrical media.

For the first test, radiative transfer results for isothermal, absorbing, emitting, and isotropically scattering two-layer slabs with transparent boundaries are studied. To simulate a slab, the emission path code uses a cylinder with a diameter D that is very large relative to its height L ($D/L = 4000$). The slabs are constructed of two sublayers with differing values of extinction coefficient ($\beta = \sigma + a$) and/or albedo ($\omega = \sigma/\beta$). Exact values of slab reflectivity and transmissivity, from which emissivity may be derived, are provided in studies by Özisik and Shouman [31] and Shouman and Özisik [32]. A large number of comparisons were performed between these emissivity

values and those computed by the emission path code. Generally, the computed emissivities were accurate to three significant digits with a relative uncertainty (99% confidence interval) of less than $\pm 0.8\%$. Although the number of tracking bundles differed for each run, seven or eight iterations with 10 000 bundles were typical. For all runs, the exact values from Özisik and Shouman lay within the predicted 99% confidence interval.

The second test case involves a nonhomogeneous, absorbing, emitting, and isotropically scattering slab which is also nonisothermal. The properties within the slab are illustrated in Fig. 4. The computed radiative fluxes at the transparent boundaries from the emission path code are compared below to values returned by the forward (conventional) MC code:

$z = 0$

emission path code: $q = 53\,974 \pm 292\ \mathrm{W\,m^{-2}}$

forward MC code: $q = 53\,872 \pm 568\ \mathrm{W\,m^{-2}}$

$z = L$

emission path code: $q = 88\,162 \pm 503\ \mathrm{W\,m^{-2}}$

forward MC code: $q = 87\,803 \pm 763\ \mathrm{W\,m^{-2}}$.

These ranges identify a 99% confidence interval. In each case, the average value from the emission path code lies within the predicted confidence interval from the forward MC code.

Several tests involving cylindrical media were also performed. Thynell and Özisik [33] provide values of the emitted flux from an absorbing, emitting, and isotropically scattering infinite cylinder with a radially varying radiative source. The emitted flux at the cylinder's boundary was computed using the emission path code for various values of β and ω and compared to results reported in the above study. The computed fluxes differed from the reported values by less than 0.4%. Also, for each case, the reported value fell within the computed 99% confidence interval, which indicated a relative uncertainty of less than $\pm 1.2\%$ (usually less than $\pm 0.75\%$).

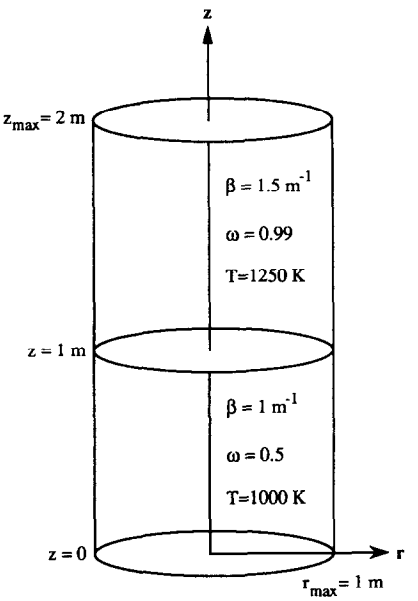

FIG. 5. Properties within the finite test cylinder.

Two other tests were performed using finite, nonhomogeneous, nonisothermal cylinders with an isotropically scattering constituent, and comparisons were made between boundary fluxes computed via the emission path code and those computed via the forward MC code. Since the results of the two tests are similar, only the first is described here. The properties within the finite test cylinder are identified in Fig. 5. In Fig. 6, the radiative fluxes q at the $z = 0$ and z_{max} planes are plotted as a function of radius. The radiative flux at various axial locations is plotted in Fig. 7. To indicate the influence of scattering, the fluxes that result if scattering is removed ($\sigma = 0$) are computed with the forward MC code and are also plotted in Figs. 6 and 7. Error bars are not included in the figures since they are indistinguishable from the plot symbols. Note that the results from the forward MC code are represented by lines rather than individual

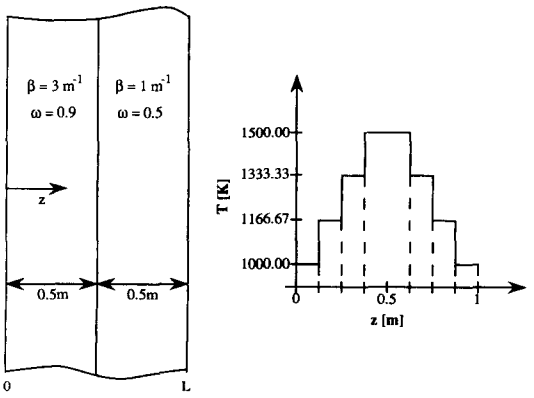

FIG. 4. Properties within a nonhomogeneous, nonisothermal slab with transparent boundaries.

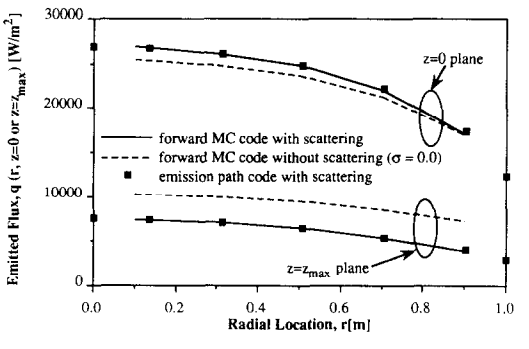

FIG. 6. Emitted fluxes for scattering and nonscattering conditions at the $z = 0$ and z_{max} boundaries for the finite test cylinder.

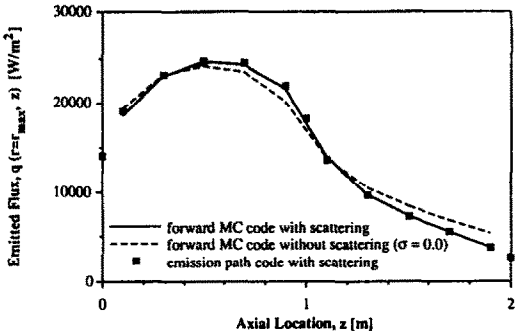

FIG. 7. Emitted fluxes for scattering and nonscattering conditions at the $r = r_{max}$ boundary for the finite test cylinder.

symbols to indicate that these results apply over finite area elements (five radial disks at each end and ten axial bands) not at specific radial or axial locations. Also, because the forward MC results apply as average values over a finite area, they do not exactly match the emission path results, which apply at precise locations. Nonetheless, the results from the two codes agree very well.

Nonhomogeneous scattering results

The success of the collection of test cases provided above serves to validate the operation of the reverse MC code. Now, to demonstrate an application to nongray media, a sample case is presented involving a nonhomogeneous, nonisothermal, cylindrical mixture of isotropically scattering, gray particles and a real gas (CO_2). The boundary is taken to be transparent. Because the scattering particles are gray, the flux to a specific area element dA on the boundary is computed using a single set of emission paths. That is, the paths are valid for all wavelengths and a block transmissivity formulation [13] is used to evaluate the gas–particle path intensity needed in equation (19). Although equation (19) is written in terms of a spectral calculation for q_λ, the same equation applies for evaluating the total flux q if the subscript λ is removed from all quantities.

The axisymmetric medium investigated is a cylinder that is uniform in the axial direction with length $z_{max} = 3$ m and radius $r_{max} = 0.5$ m. While the scattering albedo of the particle is fixed at $\omega = 0.99$, the extinction coefficient β of the particulate and temperature T vary with radius r as described in Fig. 8. The distributions for β and T were chosen to demonstrate the effect of shielding by an optically thick cold region near the wall and to emphasize the necessity for proper consideration of nonhomogeneities. Because the emission path code requires a homogeneous cell structure in describing the medium, the boundary layer region is approximated with five uniform concentric volume elements. The gaseous constituent is CO_2 at a uniform pressure of 1 atm. The total emitted flux q of the gas–particle medium is plotted for precise locations along the $z = 0$ (or z_{max}) boundary in Fig. 9 and for locations along the $r = r_{max}$ boundary in Fig. 10. Also included is a 99% confidence interval for each computed value, although the error bars are usually indistinguishable.

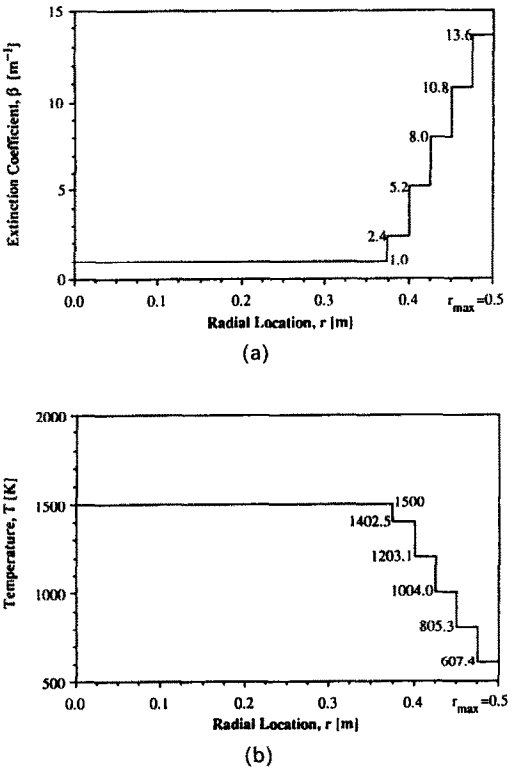

FIG. 8. The radial distributions of extinction coefficient and temperature within the axially uniform cylindrical medium. (Values shown on the graphs are the specific values at each step.) (a) Extinction coefficient. (b) Temperature.

For comparison, the emitted fluxes for two other cases are included in Figs. 9 and 10. The first involves the fluxes that result if scattering is neglected. That is, the particle scattering coefficient σ is set to zero while retaining the original values of particle absorption coefficient a and temperature T, obtainable from Fig.

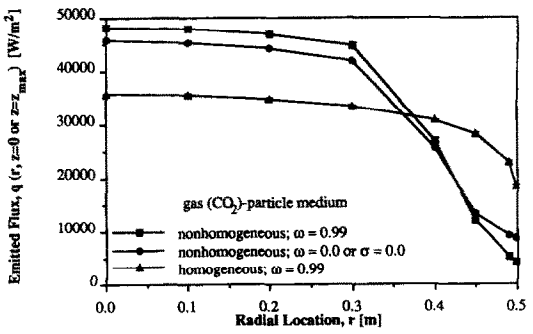

FIG. 9. Emitted fluxes at the $z = 0$ or z_{max} boundary of an axially symmetric cylindrical medium (shown in Fig. 8) containing a gas (CO_2) and particles.

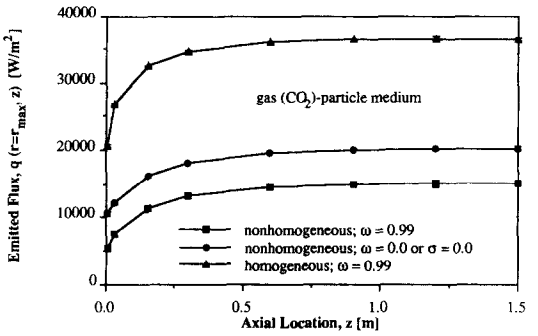

FIG. 10. Emitted fluxes at the $r = r_{max}$ boundary of an axially symmetric cylindrical medium (shown in Fig. 8) containing a gas (CO_2) and particles.

8. The original gas properties are also retained. Thus, the effect of the optically thick scattering region near the sides of the cylinder can be investigated. The second case involves the fluxes from a homogeneous medium with a volume-averaged temperature

$$T_{ave} = \left[\frac{z_{max} \int_0^{r_{max}} [T(r)]^4 2\pi r \, dr}{\pi r_{max}^2 z_{max}} \right]^{1/4} \quad (21)$$

and average particle extinction coefficient

$$\beta_{ave} = \frac{\int_0^{r_{max}} \beta(r) \, dr}{r_{max}} . \quad (22)$$

The scattering albedo retains its value of 0.99, and the gas conditions are unchanged. By comparing the emitted flux from this homogeneous cylinder with that of the original medium, the importance of properly accounting for nonhomogeneities is demonstrated.

Several important observations follow. First, for the gas–particle emitted flux in Figs. 9 and 10, note that at the base ($z = 0$ plane in Fig. 9), the flux is very high for the nonhomogeneous, $\omega = 0.99$ case. The implication is that the high degree of scattering near the side walls acts like a reflecting boundary, channeling core emission to the base planes. Nearer the corners ($r = r_{max}$ and $z = 0$) and on the sides ($r = r_{max}$), scattering in the optically thick region adjacent to the sides acts as a shield, obstructing the view of the hot core. When scattering is removed from the medium (the nonhomogeneous, $\omega = 0$ case), the shielding due to scattering is absent and emission to the side walls and corners increases, as seen in Figs. 9 and 10. Near the center of the base, the emission is reduced from that of the scattering case since the channeling effect noted above is removed and core emission can escape the medium in any direction. The results from the homogeneous case illustrate the importance of accurately describing the true nonhomogeneous nature of the medium. The emitted flux for all locations around the cylinder differs greatly from the nonhomogeneous, $\omega = 0.99$ results, despite the use of reasonable average values for β and T. Apparently, under the assumption of homogeneity, the core temperature is reduced, which directly reduces the emission to the center of the base. Near the corners and on the sides, the emission is increased over both nonhomogeneous cases, probably because the temperature of the region adjacent to the side walls is much greater. Self-absorption of energy emitted by the gas in the core by gas in the cold boundary region is not a factor for the homogeneous medium.

4. CONCLUSIONS

The concept of the emission path has been introduced. This concept can be viewed as an extension of the line-of-sight to scattering, reflecting media with arbitrary scattering phase functions and arbitrary bidirectional reflectivities at surface elements. Because the path length basis for the method allows the rigorous incorporation of length-dependent gas-band models, exact calculations of emission (flux or intensity) are possible for multidimensional, nonhomogeneous, nonisothermal media with reflecting boundaries and which contain mixtures of gases and particles (or other nongaseous constituents). More fundamentally, the emission path provides an alternative way of viewing emission from scattering, reflecting media. That is, emission can be considered as a path phenomenon rather than a volumetric one. For radiative emission in participating media, this interpretation leads to the definition of meaningful characteristic lengths, such as those introduced by Walters and Buckius [34, 35].

Another strength of the reverse Monte Carlo (emission path) method is its computational efficiency and excellent variance characteristics. Every bundle path contributes to the desired result, and the reverse tracing technique implicitly identifies those volume and surface elements that are radiatively significant. By contrast, forward (conventional) MC solutions require the emission of photon bundles from everywhere within the enclosure with only a small fraction contributing to the radiative transfer value evaluated at a particular detector element. Thus, in computing the emission over the entire boundary of a medium and at selected internal locations to a given level of precision, it is arguable that the reverse approach requires less computation time than the forward. The forward solution may lead to a large fraction of emitted bundles being collected within relatively few area elements, with all other elements receiving very few bundles. Because a result's precision is related to the number of bundles which contribute to it, the emission value at an element that receives few bundles will have a large variance. The reverse approach, on the other hand, has the advantage of requiring no more and no less bundles than necessary at each detector location since the locations are treated individually.

The emission path concept has clear applicability to many studies involving participating media. For

example, computer graphics applications which involve participating media are quite compatible with the emission path concept since in many respects it is a logical extension of the ray-tracing algorithms commonly used. For many radiative heat transfer problems, the emission path approach may be too computationally time consuming. Yet, in providing a technique able to rigorously incorporate path length-dependent gas-band models into problems involving scattering and boundary reflection, the approach is both significant and useful.

REFERENCES

1. K. M. Case, Transfer problems and the reciprocity principle, *Rev. Mod. Phys.* **29,** 651–663 (1957).
2. H. R. Gordon, Ship perturbation of irradiance measurements at sea. 1: Monte Carlo simulations, *Appl. Opt.* **24**(23), 4172–4182 (1985).
3. D. G. Collins, W. G. Blättner, M. B. Wells and H. G. Horak, Backward Monte Carlo calculations of the polarization characteristics of the radiation emerging from spherical-shell atmospheres, *Appl. Opt.* **11**(11), 2684–2696 (1972).
4. C. N. Adams and G. W. Kattawar, Radiative transfer in spherical shell atmospheres—I. Rayleigh scattering, *Icarus* **35,** 139–151 (1978).
5. J. F. Blinn, Light reflection functions for simulation of clouds and dusty surfaces, *Comput. Graphics* **16**(3), 21–29 (1982).
6. J. T. Kajiya and B. P. Von Herzen, Ray tracing volume densities, *Comput. Graphics* **18**(3), 165–174 (1984).
7. T. Nishita, Y. Miyawaki and E. Nakamae, A shading model for atmospheric scattering considering luminous intensity distribution of light sources, *Comput. Graphics* **21**(4), 303–310 (1987).
8. P. Sabella, A rendering algorithm for visualizing 3D scalar fields, *Comput. Graphics* **22**(4), 51–58 (1988).
9. D. K. Edwards, Numerical methods in radiation heat transfer, *Proc. Second National Symp. on Numerical Properties and Methodologies in Heat Transfer* (Edited by T. M. Shih), pp. 479–496. Hemisphere, Washington, DC (1983).
10. J. E. Reardon *et al.*, ASRM radiation and flowfield prediction status, *19th JANNAF Exhaust Plume Technology Subcommittee Meeting*, Redstone Arsenal, Alabama, 13–16 May, pp. 537–547 (1991).
11. H. F. Nelson, Modeling for rocket plume base heating calculations, *19th JANNAF Exhaust Plume Technology Subcommittee Meeting*, Redstone Arsenal, Alabama, 13–16 May, pp. 585–593 (1991).
12. R. M. Goody, *Atmospheric Radiation*—I. *Theoretical Basis*. Oxford University Press, London (1964).
13. D. K. Edwards, Molecular gas band radiation. In *Advances in Heat Transfer* (Edited by T. F. Irvine and J. P. Hartnett), Vol. 12, pp. 115–193. Academic Press, New York (1976).
14. R. Viskanta and M. P. Mengüc, Radiation heat transfer in combustion systems, *Prog. Energy Combust. Sci.* **13,** 97–160 (1987).
15. M. P. Mengüc and R. Viskanta, An assessment of spectral radiative heat transfer predictions for a pulverized coal-fired furnace, *Heat Transfer 1986, Proc. Eighth Int. Heat Transfer Conf.*, San Francisco, California, Vol. 2, pp. 815–820 (1986).
16. W. H. Irvine, The formation of absorption bands and the distribution of photon optical paths in a scattering atmosphere, *Bull. Astron, Inst. Neth.* **17**(4), 266–279 (1964).
17. R. O. Buckius and A. Fernandez-Fraga, The optical path length approach to radiation heat transfer with isotropic scattering and gaseous absorption, *J. Quant. Spectrosc. Radiat. Transfer* **24,** 1–13 (1980).
18. R. D. Skocypec and R. O. Buckius, Photon path length analysis of radiative transfer in planar layers with arbitrary temperature distributions, *J. Quant. Spectrosc. Radiat. Transfer* **35,** 109–120 (1986).
19. R. D. Skocypec and R. O. Buckius, Photon path length analysis of radiative transfer in planar layers with single internal sources, *J. Quant. Spectrosc. Radiat. Transfer* **35,** 87–108 (1986).
20. R. D. Skocypec, D. V. Walters and R. O. Buckius, Total hemispherical emittances for isothermal mixtures of combustion gases and scattering particulate, *Combust. Sci. Technol.* **47,** 239–252 (1986).
21. G. H. Watson and A. L. Lee, Thermal radiation model for solid rocket booster plumes, *J. Spacecraft* **14**(11), 641–647 (1977).
22. F. R. Steward and K. H. Guruz, Radiative heat transfer in absorbing, emitting, and scattering media using the Monte Carlo method, *Trans. CSME* **3,** 10–16 (1975).
23. L. W. Stockham and T. J. Love, Radiative heat transfer from a cylindrical cloud of particles, *AIAA J.* **6,** 1935–1940 (1968).
24. R. P. Gupta, T. F. Wall and J. S. Truelove, Radiative scatter by fly ash in pulverized-coal-fired furnaces: application of the Monte Carlo method to anisotropic scatter, *Int. J. Heat Mass Transfer* **26,** 1649–1660 (1983).
25. D. K. Edwards, Hybrid Monte-Carlo matrix-inversion formulation of radiation heat transfer with volume scattering, *23rd ASME/AIChE National Heat Transfer Conf.*, Denver, Colorado, 4–7 August, HTD-Vol. 45, pp. 273–278 (1985).
26. D. K. Edwards and D. S. Babikian, Volume interchange factors for hypersonic vehicle wake radiation, *AIAA 22nd Thermophysics Conf.*, Honolulu, Hawaii, 8–10 June, AIAA Paper 87-1520 (1987).
27. D. K. Edwards, Y. Sakurai and D. S. Babikian, Examination of an alternative to the Bobco plume radiation model, *AIAA 20th Thermophysics Conf.*, Williamsburg, Virginia, 19–21 June, AIAA Paper 85-1069 (1985).
28. D. K. Edwards and D. S. Babikian, Radiation from a nongray scattering, emitting, and absorbing solid rocket motor plume, *J. Thermophys. Heat Transfer* **4**(4), 446–453 (1990).
29. C. B. Ludwig, W. Malkmus and J. Walker, The standard infrared radiation model, *AIAA 16th Thermophysics Conf.*, Palo Alto, California, 23–25 June, AIAA Paper 81-1051 (1981).
30. S. T. Thynell, Radiation due to CO_2 or H_2O and particles in cylindrical media, *J. Thermophys. Heat Transfer* **4**(4), 436–445 (1990).
31. M. N. Özisik and S. M. Shouman, Source function expansion method for radiative transfer in a two-layer slab, *J. Quant. Spectrosc. Radiat. Transfer* **24,** 441–449 (1980).
32. S. M. Shouman and M. N. Özisik, Radiative transfer in an isotropically scattering two-region slab with reflecting boundaries, *J. Quant. Spectrosc. Radiat. Transfer* **26,** 1–9 (1981).
33. S. T. Thynell and M. N. Özisik, Radiative transfer in absorbing, emitting, isotropically scattering, homogeneous cylindrical media, *J. Quant. Spectrosc. Radiat. Transfer* **38,** 413–426 (1987).
34. D. V. Walters and R. O. Buckius, On the characteristic lengths for absorbing, emitting, and scattering media, *Int. J. Heat Mass Transfer* **33,** 805–813 (1990).
35. D. V. Walters and R. O. Buckius, Mean emission length approach to multidimensional radiative transfer including scattering and real gas absorption, *Int. J. Heat Mass Transfer* **35,** 131–140 (1992).